Reaction mechanisms of fast neutrons on ^{51}V below 21 MeV

P. Reimer,[1,2] V. Avrigeanu,[1,3] A. J. M. Plompen,[1,*] and S. M. Qaim[2]
[1]*European Commission, Joint Research Centre, Institute for Reference Materials and Measurements, Retieseweg, B-2440 Geel, Belgium*
[2]*Institut für Nuklearchemie, Forschungszentrum Jülich GmbH, D-52425 Jülich, Germany*
[3]*"Horia Hulubei" National Institute for Physics and Nuclear Engineering, P.O. Box MG-6, 76900 Bucharest, Romania*
(Received 5 June 2001; published 3 December 2001)

Cross sections of the $^{51}V(n,p)^{51}Ti$, $^{51}V(n,\alpha)^{48}Sc$, and $^{nat}V(n,x\alpha)^{47}Sc$ reactions were measured in the energy range from 11.7 to 20.5 MeV. The measurements for the latter reaction establish for the first time a consistent excitation curve. The present data for the (n,p) process connect the measurements around 14 MeV with the recent data set above 17 MeV. The shapes and magnitudes of the three excitation functions from the reaction thresholds up to 21 MeV, as well as the ones for the competing reaction channel $^{51}V(n,2n)^{50}V$, are described by model calculations using a consistent parameter set. The agreement between experimental and calculated data is, in general, good both at the maxima and at the tails of the excitation functions. In contrast to earlier studies, the major contribution to the $^{nat}V(n,x\alpha)^{47}Sc$ cross section at 14.8 MeV incident energy is attributed to the $^{50}V(n,\alpha)^{47}Sc$ reaction; at energies above 15 MeV the $^{51}V(n,n'\alpha)$ process is dominant.

DOI: 10.1103/PhysRevC.65.014604 PACS number(s): 24.10.−i, 24.60.Dr, 25.40.−h, 28.20.−v

I. INTRODUCTION

Measured data of fast-neutron induced reaction cross sections are of considerable interest in testing nuclear models. Relatively few measurements have been done above the incident energy of 15 MeV and the scatter around 14 MeV is often large [1,2]. Here, new measurements are presented for the $^{nat}V(n,x\alpha)^{47}Sc$ and $^{51}V(n,\alpha)^{48}Sc$ reactions between 11.7 and 20.5 MeV, and for the $^{51}V(n,p)^{51}Ti$ reaction at 15 and 16.1 MeV. The new data for the $^{nat}V(n,x\alpha)^{47}Sc$ reaction are the first that establish an excitation curve over this energy range which is consistent with nuclear models.

With the new measurements vanadium is now an excellent test case for nuclear models in the neutron energy range up to 20 MeV. Experimental results are not only available for the above-mentioned reaction channels but also for the total cross section, elastic, and inelastic scattering cross sections, and the $^{51}V(n,2n)^{50}V$ cross section [3–8]. Measured emission spectra for protons, neutrons, and alphas are available around 14.5 MeV [9,10]. In addition, *s*-wave resonance spacing information is available from neutron and proton induced reactions [11,12].

The second part of this work explores the possibility of describing the new and the existing experimental information up to 20 MeV with a consistent set of parameters. To account for the reaction channels that are open the direct, preequilibrium (PE) and statistical processes should be considered. Among them, PE emission is important for the description of the data of the (n,x) reactions in the energy range 15–21 MeV. This is demonstrated here in the context of the geometry dependent hybrid model (GDH). One may note that PE emission becomes more important at higher energies, e.g., for development of accelerator-driven systems (ADS) [13]. Therefore any improved understanding of PE processes in the energy the range of 15–21 MeV will be useful in making the higher energy calculations more reliable.

The modeling of the present work concentrates on a good description of the neutron-induced reactions on vanadium within the approach outlined above. No analysis was attempted of experimental data for similar reaction channels on neighboring nuclei, such as the (n,α) reactions on ^{48,50}Ti and ^{54}Cr [1,14].

Vanadium alloys have long been considered as fusion-reactor structural materials for their low-activation properties. Structural materials studied for fusion reactors are now also being considered for ADS. Since gas inclusions are detrimental to mechanical stability, a good knowledge of gas producing reactions like $^{51}V(n,\alpha)^{48}Sc$, $^{nat}V(n,x\alpha)^{47}Sc$, and $^{51}V(n,p)^{51}Ti$ is needed [15]. A particular problem that emerged recently concerned the measured activity of ^{47}Sc in vanadium alloys that were irradiated with fast neutrons of energies characteristic for a fusion reactor. These measured activities were much less than those predicted by a (renormalized) model estimate of the $^{nat}V(n,x\alpha)^{47}Sc$ cross section. This triggered the present measurements since the existing experimental information for this reaction was inconsistent and could not be used to resolve the discrepancy [16].

The measurements are described in Sec. II. The main assumptions involved in the PE and Hauser-Feshbach (HF) statistical model calculations and the parameters chosen are discussed in Sec. III. The experimental data and their interpretation are discussed in detail in Sec. IV. The conclusions of the work are given in Sec. V.

II. EXPERIMENTAL METHOD

Measured cross sections were determined by the well known activation method. Two different experimental facilities were used to perform the irradiations. The irradiation at 11.7 MeV was performed in Jülich while the energy range from 13.4 to 20.5 MeV was covered with irradiations done in Geel. The method that was applied closely follows that detailed in Ref. [2] in the case of the Geel irradiations and in Ref. [1] in the case of the Jülich irradiation.

*Corresponding author. Email address: arjan.plompen@irmm.jrc.be

A. Samples and irradiations

Samples consisted of natural vanadium with an isotopic composition of 0.25% ^{50}V and 99.75% ^{51}V [17]. The samples were prepared by punching discs of 10 and 13 mm diameter and 350–450 μm thickness from metallic vanadium sheets. One to four of those were sandwiched between two Al foils of the same diameter for neutron flux monitoring. Additional Fe, Nb, and Ni foils were also attached in order to check the results from the Al monitors.

At the variable-energy Compact-Cyclotron CV-28 at FZ Jülich, an irradiation with quasi-mono-energetic neutrons of 11.7 MeV was performed using the ^{2}H$(d,n)^{3}$He reaction ($Q=3.269$ MeV) with a D_2 gas target (DD neutron field). The details of the neutron source are described in Refs. [18,19]. The samples were mounted together with the reference foils at 1 cm distance from the end of the beamstop. The irradiation was done in the 0° direction relative to the beam with a deuteron energy of 9 MeV and a beam current of about 4 μA. In order to be able to correct for background neutrons from interactions of the deuterons with structural material of the gas cell two irradiations were necessary. One was performed with a filled cell (gas in) and one with an empty cell (gas out), but otherwise with exactly the same geometry and beam conditions. The beam current was recorded with a charge integrator.

Measurements between 13.4 and 20.5 MeV were performed at the 7 MeV Van de Graaff accelerator in Geel using the ^{3}H$(d,n)^{4}$He reaction ($Q=17.59$ MeV) with a solid-state Ti/T target (1.923 mg/cm^2 thick) on a silver backing (DT neutron field). For energies above 16 MeV the samples were irradiated in the 0° direction at 1 cm distance using deuteron beams of 1, 2, 3, and 4 MeV. The angular distribution of the DT neutron source reaction was used to cover the energy region between 13.4 and 16.3 MeV. The samples were irradiated at angles between 65° and 120° relative to the deuteron beam and a distance of about 3–4 cm between the center of the target and the front of the sample. A longcounter operated in multichannel-scaling acquisition mode was used to record the time profile of the neutron flux during the experiment. Corrections for time-dependent fluctuations are made following Ref. [2].

B. Mean neutron energy and background fluence

The Monte Carlo program NEUT_HAV [20,21] was used to calculate the average neutron energy and the neutron spectrum for each sample in the DD neutron field. This code takes into account the energy loss, energy spread, and angular straggling of the deuterons in the entrance window of the cell, the neutron production within the volume of the gas cell, the angular distribution of the ^{2}H$(d,n)^{3}$He reaction, the breakup of the deuterons in the D_2 gas according to the results from Ref. [22], and the activation geometry. The main DT neutron spectrum and the low energy background resulting from multiple scattering in the Geel irradiations were calculated with the Monte Carlo code MCNP [23], taking into account the sample geometry, the TiT target and silver backing, the last part of the beamtube and the sample holder (Al). The neutron source description that was input in these calculations was determined with the aid of the program KINEMA that is based on the reaction tables of Ref. [24] and the stopping powers of Ref. [25]. Corrections for multiple scattering are maximum at 4 MeV incident deuteron energy and in that case amount to 7% for the ^{58}Ni$(n,p)^{58}$Co and less than 2% for the remaining reactions.

The well-known monitor reaction ^{27}Al$(n,\alpha)^{24}$Na [26] was used to determine the neutron fluence for the (n,α) and $(n,n'\alpha)$ cross section measurements. In the case of the (n,p) reaction, where the irradiation time was too short to build up enough ^{24}Na activity, the ^{27}Al$(n,p)^{27}$Mg reaction was used as reference. After this short irradiation a second run was performed under the same beam conditions and with the same sample geometry, but long enough to build up enough activity from the ^{27}Al$(n,\alpha)^{24}$Na reaction. Using the longcounter for normalization the flux could be extrapolated for the short run. The flux values from both reactions agreed within the uncertainties.

The ^{56}Fe$(n,p)^{56}$Mn and ^{93}Nb$(n,2n)^{92m}$Nb reactions were used together with time of flight measurements (TOF) to correct for low energy neutrons originating from the target (Geel irradiations [27]). For the experiment at Jülich also the D(d,pn) breakup reaction had to be taken into account, which is the only remaining substantial source of low-energy neutrons after application of the gas-in/gas-out procedure [28]. The corrections are readily calculated based on the well-known spectrum (see above).

Both in the Geel and Jülich cases, the corrections for background neutrons require excitation curve shape data. These are taken from experimental data supplemented with STAPRE calculations.

The magnitude of the corrections for low energy neutrons in the case of the DT field increases with incident deuteron energy and depends on the threshold of the reaction. The correction for Nb was negligible, while it was up to 50% for Ni. For the ^{27}Al$(n,\alpha)^{24}$Na reference reaction a maximum correction of 15% had to be applied for 4-MeV deuteron energy. In the case of the vanadium reactions this correction was less than 2% due to the higher effective reaction thresholds for the ^{nat}V$(n,x\alpha)^{47}$Sc and ^{51}V$(n,\alpha)^{48}$Sc reactions and due to the absence of large low energy neutron contributions for the present measurements in the case of the ^{51}V$(n,p)^{51}$Ti reaction. In the case of the DD field the correction for breakup neutrons was negligible.

C. Measurement of radioactivity

Standard γ-ray spectroscopy was employed for the measurement of the radioactivity. Three lead-shielded HPGe detectors were used which were connected to personal computer data acquisition systems via separate analog-to-digital converters (ADC's). The detectors in Jülich were controlled with the software GAMMAVISION supplied by EG&G Ortec whereas in Geel the S100 system of Canberra was used. To obtain maximum counting statistics, the monitor foils were placed directly on the detector cap. For all detectors the photopeak efficiency was determined using calibrated standard sources, supplied by PTB, Braunschweig, Germany and DAMRI, Gif-sur-Yvette, France. An analytical function [29]

TABLE I. Decay data of measured reaction products (taken from Ref. [31]). All products show 100% β^- decay.

Reaction product	Half-life	Reaction	Q value (MeV)	γ-ray energy (keV)	γ-ray abundance (%)	Summing correction
^{47}Sc	3.3492(6)d	^{51}V$(n,n'\alpha)$	−10.291	159.4	68.3(4)	1
		^{50}V(n,α)	0.761			
^{48}Sc	43.67(9)h	^{51}V(n,α)	−2.058	175.4	7.48(10)	2.31(13)
				983.5	100.1(6)	1.56(7)
				1037.5	97.6(7)	1.56(7)
				1312.1	100.1(7)	1.66(7)
^{51}Ti	5.76(1) min	^{51}V(n,p)	−1.688	320.1	93.1(4)	1.0024[a]

[a]Taken from Ref. [2].

was used to describe the measured calibration points. Since corrections for coincidence summing effects were needed for some cases the total efficiency was determined as well [30]. In the case of ^{48}Sc the summing corrections were checked experimentally and for ^{51}Ti taken from the literature [2]. The values are summarized in Table I. Further corrections were applied for γ-ray abundance, γ-ray self-absorption, and the sample geometry.

III. NUCLEAR MODEL CALCULATIONS

Often, experimental data do not impose sufficient constraints on the PE and HF statistical models. Most data could be reproduced equally well in terms of different approaches by adjustment of parameters, even of so-called ''parameter free'' models [32]. This is due to the different treatment of the *special* PE parameters and the *external* ones which describe general nuclear quantities [33]. In order to diminish these effects we have looked for a consistent set of external parameters based on different types of independent experimental data. A second point of model consistency lies in the use of the same model parameters for the description of the various processes in the framework of the direct interaction, pre-equilibrium, and compound-nucleus statistical models.

A. Nuclear models

1. Direct inelastic scattering

Neutron inelastic scattering is the only direct interaction which is taken into account. The distorted wave Born approximation (DWBA) has been used to describe neutron direct inelastic scattering on the discrete excited levels of the target nucleus, with the computer code DWUCK4 [34]. The weak coupling model was adopted for the odd nucleus ^{51}V using the excitation energies of the first 2^+, 3^-, and 4^+ levels of ^{50}Ti [35], and the corresponding deformation parameter values of 0.15, 0.09, and 0.15.

2. Preequilibrium emission

The PE cross sections have been calculated with the generalized version [36] of the geometry-dependent hybrid (GDH) model [37], which includes α-particle emission, angular-momentum conservation (computer code STAPRE-H95 [38]), and a revised formula for the particle-hole level density $\rho(p,h,E)$ (subroutine PLD [39,40]). Here GDH intranuclear transition rates are calculated on the basis of the average imaginary optical-model potential (OMP). The only free parameter is the α-particle preformation probability. For this quantity a value of 0.25 was taken from systematics for this A range [41].

3. Equilibrated statistical emission

The nucleon, α-particle, and γ-ray-emission by equilibrated excited nuclei were described with the statistical Hauser-Feshbach model following Uhl [42]. The optical-model transmission coefficients have been calculated by the code SCAT2 [43].

The level density description was split in four excitation energy regions. In region I, discrete levels were used from the ground state to an excitation energy E^* of E_d. In region II from $E^*=E_d$ to the neutron binding energy $E^*=B_n$ the back-shifted Fermi-gas model was used [44]. In region IV above $E^*=15$ MeV, the washing out of shell effects was treated with the well-known expression (see, e.g., Ref. [45]). In region III between $E^*=B_n$ and 15 MeV, a smooth transition is made between regions II and IV.

B. Model parameters

1. OMP parameters

For the neutron channel a local OMP parameter set was used in the calculation. The starting point was Eq. (7) of Ref. [4] which gives an accurate description of the resonance data and the neutron total cross section data available at that time (SPRT method [46]). Meanwhile new high-resolution neutron total cross sections have become available [6]. These data, averaged over 200-keV intervals are compared to other experimental data [4,47] and with the optical models of Ref. [4] and of this work in Fig. 1. The OMP of the present work improves the description of the minimum between 0.5 and 1 MeV, the maximum around 3 MeV, and the decrease above 8 MeV by a small change of the imaginary-potential diffuseness of the OMP of Ref. [4],

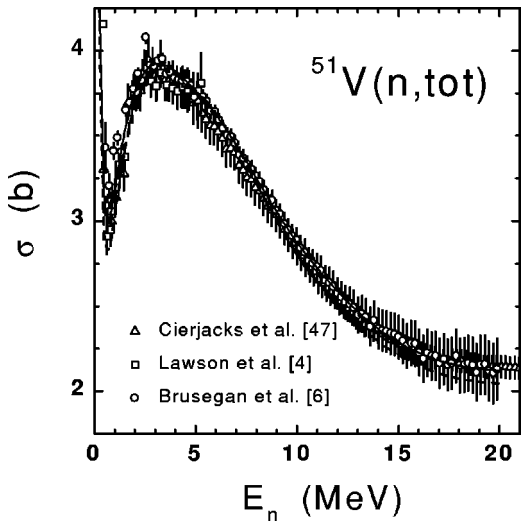

FIG. 1. Comparison of experimental and calculated total cross sections of vanadium, by using the OMP parameter set given by Eq. (7) of [4] (dashed curve) and including the presently modified a_W (solid curve). The experimental data are averaged over a 200-keV interval.

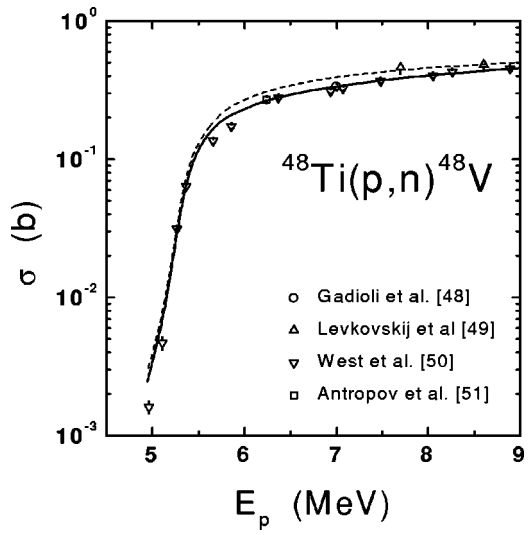

FIG. 2. Comparison of the measured and calculated reaction cross sections for the reaction ^{48}Ti$(p,n)^{48}$V in the energy range above the threshold by using the OMP parameter sets of Hetrick *et al.* [54] for proton energies below 5 MeV, and the global parameter set of Kailas *et al.* for higher energies [52] (solid curve), as well as the latter parameter set over the whole energy range (dashed curve).

$$a_W = \begin{cases} 0.24+0.05E, & E \leqslant 4 \text{ MeV}, \\ 0.20+0.06E, & 4 \leqslant E \leqslant 6.2 \text{ MeV}, \\ 0.76-0.029E, & 6.2 \leqslant E \leqslant 10 \text{ MeV}, \\ 0.47, & E \geqslant 10 \text{ MeV}. \end{cases} \quad (1)$$

The corresponding *s*-wave strength function value $S_0 = 6.1 \times 10^{-4}$ is in good agreement with the experimental value $(6.9 \pm 2.4) \times 10^{-4}$ [6].

The proton OMP was chosen by comparison of the calculated reaction cross section with the available data for the ^{48}Ti$(p,n)^{48}$V reaction in the incident energy range from 4.9 to 8.9 MeV (Fig. 2 [48–51]). The best agreement was obtained with the global parameter set of Kailas *et al.* for proton energies higher than 5 MeV [52], and the global parameter set of Perey [53] with the asymmetry dependence of Ref. [54] below 5 MeV. Use of the OMP of Kailas *et al.* in the whole energy range leads to higher (p,n) reaction cross sections due to lower *s*-wave transmission coefficients for protons below 5 MeV, i.e., in the exit channel.

The optical model potential for calculation of α-particle transmission coefficients was established previously by analysis of the experimental (n,α) reaction cross sections just above the effective Coulomb barrier [55].

Finally, the charged-particle transmission coefficients involved in this work have been checked by looking for a good description of the ^{51}V$(n,p)^{51}$Ti and ^{51}V$(n,\alpha)^{48}$Sc reaction cross sections, for energies between the threshold and $\sim$3.5 MeV above the threshold, where their effect is largest. The nuclear level density of the corresponding residual nucleus plays no role in this energy range and the preequilibrium processes are not yet present. Therefore a good description of the experimental data in this energy range validates the adopted charged-particle optical model potential (see Sec. IV).

2. Nuclear level density parameters

a. Low excitation energies. In region I, N_d discrete levels were used (see Table II). For region II the level-density parameter *a* and the back-shift Δ of the BSFG model were obtained by a fit of experimental low-lying discrete levels and average measured *s*-wave nucleon resonance spacings D_0. For nuclei without experimental *s*-wave resonance spacings the level density parameter *a* at the binding energy was obtained using the smooth curve method [56] and the available experimental information for nuclei with $41 < A < 58$. The above determination of *a* and Δ was done after the model for the moment of inertia was fixed and the result is given in Table II.

For the moment of inertia *I*, recent analyses [57,58] prefer half the rigid rotor moment I_r (we assume $r_0 = 1.25$ fm). In the case of ^{51}V experimental *s*-wave resonance spacings D_0^p [11] and D_0^n [12] are available from proton induced reactions on ^{50}Ti and from neutron induced reactions on ^{50}V. Since the target nuclei differ by six units in spin, these resonance spacings are sensitive to the adopted moment of inertia. Following the method of Ref. [59] a value of $I/I_r = 0.75 \pm 0.06$ is obtained. Moreover, following theoretical predictions (e.g., Refs. [58,60]) we have adopted a variable ratio I/I_r that ranges from 0.5 at the ground state energy to 0.75 at the binding energy and 1 at 15 MeV, while remaining constant above.

b. High excitation energies. At excitation energies above the binding energy it is necessary to incorporate the washing out of shell effects in the level density parameters with ex-

TABLE II. Discrete-level number N_d up to excitation energy E_d [31], used in Hauser-Feshbach calculations, and the low-lying levels and *s*-wave nucleon-resonance spacings D_0^{exp} in the nucleon energy range ΔE above the respective binding energy B, for the target-nucleus ground-state spin I_0, fitted in order to obtain the BSFG level-density parameter a and ground-state shift Δ (corresponding to a spin cutoff factor calculated with a variable moment of inertia between the half and 75% of the rigid-body value, for the excitation energies from g.s. to the nucleon binding energy, and the reduced radius $r_0 = 1.25$ fm).

			Fitted level and resonance data						
Nucleus	N_d	E_d	N_d	E_d	$B+\frac{\Delta E}{2}$	I_0	D_0^{exp}	a	Δ
		(MeV)		(MeV)	(MeV)		(keV)	(MeV^{-1})	(MeV)
^{52}V	24	2.169	24	2.17	7.361	7/2	4.1±0.6 [a]	6.05	−1.55
							4.5±0.5 [b]		
^{51}V	28	3.577	28	3.58	10.646	0	7.9±0.6 [c]	5.68	−0.50
					11.071	6	2.30±0.60 [a]		
							2.15±0.27 [b]		
^{51}Ti	22	4.187	22	4.19	6.565	0	125±70 [a]	6.06	0.56
							84.8±24.4 [b]		
^{50}V	32	2.162	44	2.53				5.90	−1.88
^{50}Ti	19	4.940	19	4.94	10.059	7/2	4.00±0.80 [a]	5.55	1.20
							4.75±0.37 [b]		
^{50}Sc	15	3.510	19	3.73				5.90	0.40
^{48}Sc	28	2.811	46	3.39				5.15	−1.67
^{47}Sc	19	2.410	19	2.41				5.60	−1.35
^{47}Ca	18	4.205	18	4.20				5.10	0.20

[a]RIPL Obninsk file [12].
[b]RIPL Beijing file [12].
[c]Reference [11].

citation energy E^*. For region IV we use the analytical approach given in Ref. [45] with the following modifications. We adopt $A/9$ MeV^{-1} for the asymptotic level density parameter based on recent microscopic results around $A\sim 50$ [61] and $A\sim 100$ [62]. The shell correction energy is determined from the condition that the entropy at the binding energy $E^*=B_n$ must be continuous when determined with the BSFG model and with the expression in Ref. [45] by means of $a_{\rm eff}=S^2/(4E^*)$. This method is similar to that of Koning and Chadwick [63]. The resulting values for the shell correction energy differ by up to 2 MeV from the microscopic correction of Möller *et al.* [64]. This difference is typical of that obtained using different mass formulas [65]. The procedure followed leaves a residual discontinuity of the level density at the binding energy. The discontinuity is eliminated by interpolation in region III. Finally, in the analytic expression for a in region IV we adopted a normalization of the effective excitation energy E to the energies of the odd-A nuclei,

$$E = \begin{cases} E^* + 12/\sqrt{A}, & \text{odd-odd, } E \text{ in MeV,} \\ E^*, & \text{odd-}A, \\ E^* - 12/\sqrt{A}, & \text{even-even.} \end{cases} \quad (2)$$

IV. RESULTS AND DISCUSSION

The experimental results of this work are presented in Table III. They are shown graphically in Figs. 3, 4, and 6 together with the experimental results by others.

The main experimental contribution of this work concerns the measurement of the $^{\rm nat}$V$(n,x\alpha)^{47}$Sc cross section, which consists of contributions from the ^{51}V$(n,n'\alpha)^{47}$Sc and ^{50}V$(n,\alpha)^{47}$Sc processes. An excitation curve is established for the first time and it is in agreement with the good quality data recently measured around 14 MeV [68–71]. It also

TABLE III. Measured cross sections for the $^{\rm nat}$V$(n,x\alpha)^{47}$Sc, ^{51}V$(n,\alpha)^{48}$Sc, and ^{51}V$(n,p)^{51}$Ti reactions.

Neutron energy	Cross section (mb)		
(MeV)	$^{\rm nat}$V$(n,x\alpha)^{47}$Sc	^{51}V$(n,\alpha)^{48}$Sc	^{51}V$(n,p)^{51}$Ti
11.7±0.2	0.055±0.005	8.3±0.8	
13.4±0.1	0.094±0.010	14.1±1.2	
13.9±0.2	0.086±0.005	15.4±1.1	
14.3±0.2	0.089±0.006	14.2±1.2	
15.0±0.2	0.14±0.01	18.2±1.7	26±2
16.1±0.2			25±2
16.2±0.2	0.40±0.02	19.8±1.8	
18.0±0.1	4.0±0.2	21.1±1.8	
19.3±0.1	10.8±0.6	19.8±1.8	
20.5±0.1	17.3±1.3	14.6±1.6	

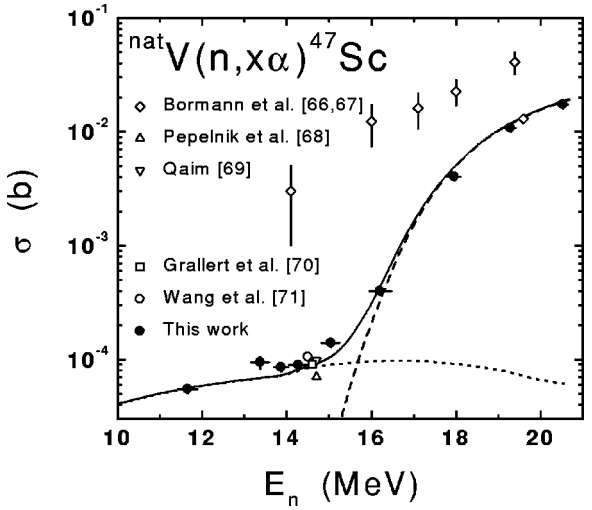

FIG. 3. Comparison of experimental and calculated excitation functions of the reaction $^{nat}V(n,x\alpha)^{47}Sc$ (solid curve). The latter was obtained as the sum of contributions of the $^{51}V(n,n'\alpha)^{47}Sc$ reaction (dashed curve) and 0.25% of $^{50}V(n,\alpha)^{47}Sc$ reaction (dotted curve). The highest energy open diamond is from Ref. [66], the remaining open diamonds are from Ref. [67].

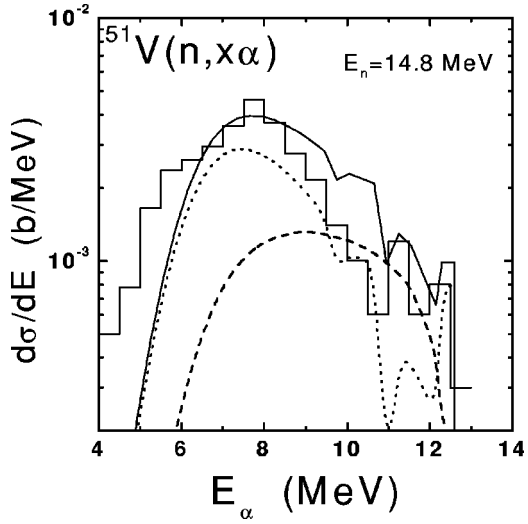

FIG. 5. Comparison of experimental [9] (histogram) and calculated (solid curve) angle integrated α-particle emission spectra from 14.8 MeV neutron-induced reactions on ^{51}V. The contributions from PE emission (dashed curve) and statistical emission (dotted curve) are shown.

shows the appropriate threshold behavior for the dominant reaction channel. Our work is at variance with the earlier data of Ref. [67]. Over the whole energy range studied here, the cross section for the production of ^{47}Sc from ^{nat}V is much lower than that suggested by this earlier measurement above 15 MeV.

Cross sections were also obtained for the $^{51}V(n,\alpha)^{48}Sc$ reaction. Above 18 MeV these provide the second measurement of this cross section. In that energy range our measurements suggest values slightly higher than those reported in Ref. [72]. This is probably due to improvements in the standard (reference) cross sections. In general, the agreement of the new measurements for the $^{51}V(n,\alpha)^{48}Sc$ reaction with the existing data is good for the given uncertainties [73].

Only two data points were added to the recent measurements by Fessler *et al.* [2] for the $^{51}V(n,p)^{51}Ti$ reaction. The energies were chosen to establish if those recent measurements should be extrapolated to the higher or the lower set of cross sections determined previously at 14 MeV. The new data agree within the uncertainties both with the results of

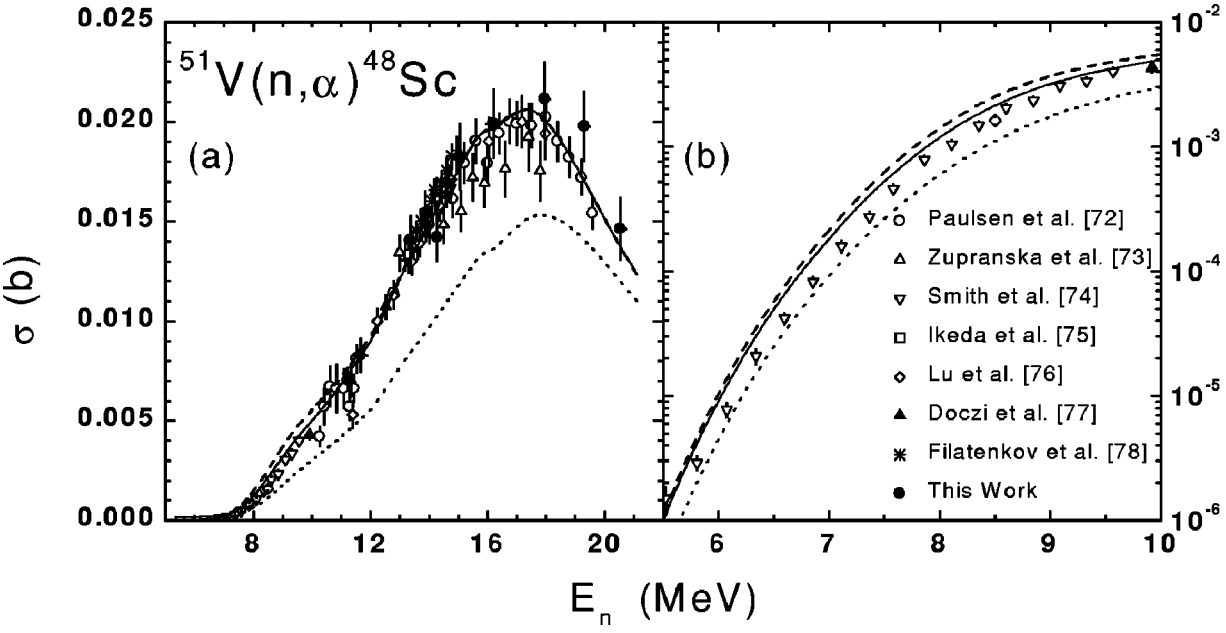

FIG. 4. Comparison of experimental and calculated excitation functions for the $^{51}V(n,\alpha)^{48}Sc$ reaction. The present model is given with the modified spin assignments to first and excited levels (solid curve), and with the spin assignments of Ref. [31] (dashed curve). Calculations with the McFadden and Satchler potential [83] are given by the dotted curves.

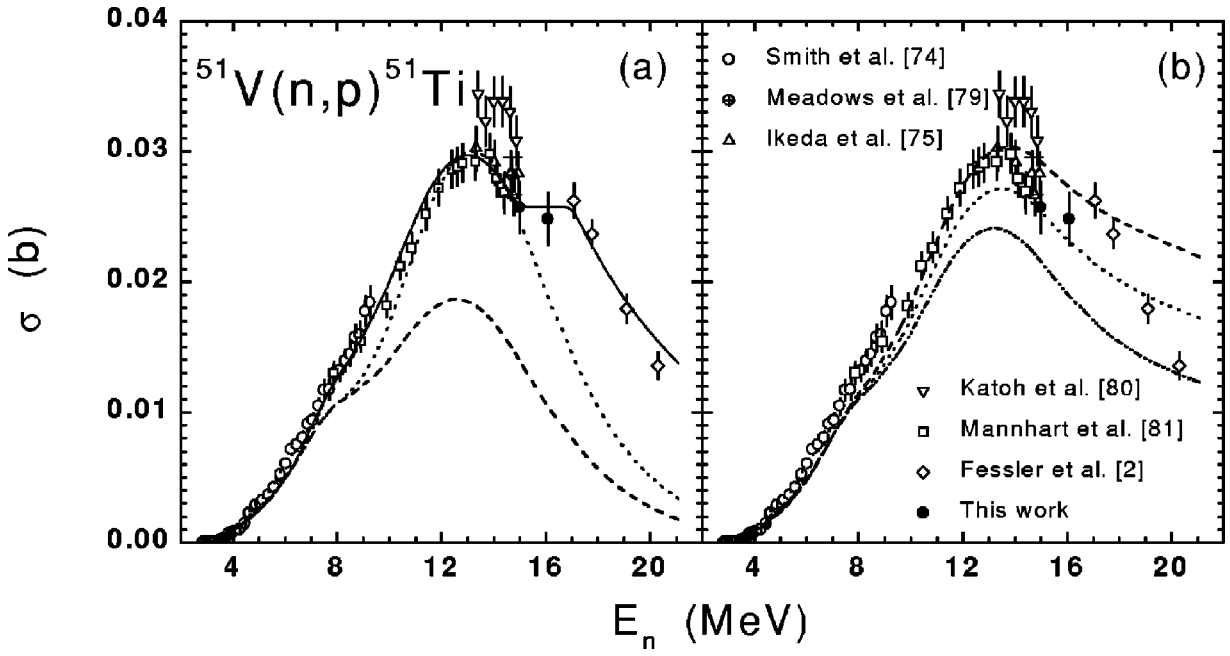

FIG. 6. (a) Comparison of experimental and calculated cross sections for the reaction $^{51}V(n,p)^{51}Ti$ by using the present model (solid curve), the pure Hauser-Feshbach statistical model (dashed curve), and the pure HF statistical model with level density parameters corresponding to a smaller average neutron-resonance spacing $D_0^n = 59$ keV (dotted curve). (b) Also shown are calculations with the exciton model with three choices for the average effective matrix element, $FM = 500$ (dashed curve), 700 (dotted curve), and 1100 MeV^3 (dash-double-dotted curve).

Fessler *et al.* [2] and with the measurements reported in Refs. [74–79,81]. A discrepancy is, however, observed with the higher cross section data of Ref. [80].

It is clear that now a firm experimental database exists for the cross sections of the dominant neutron, proton, and alpha emission channels. The only exception is the $^{51}V(n,n'p)^{50}Ti$ process. Around 14.5 MeV these data are complemented by emission spectra [9,10]. The rather complete data base suggested a careful model analysis which is compared to the data and discussed in detail in Sec. III A for the $(n,x\alpha)$ reactions, in Sec. III B for the (n,xp) reactions and in section C for the (n,xn) reactions.

A. The $(n,x\alpha)$ reactions

Clearly the trend of our new measurements for the $^{nat}V(n,x\alpha)^{47}Sc$ cross section is rather well described by the model calculation. The calculation shows that the $^{51}V(n,n'\alpha)^{47}Sc$ reaction cross section dominates above the incident energy of 15 MeV, where it is an order of magnitude higher than the cross section of the $^{50}V(n,\alpha)^{47}Sc$ reaction multiplied by the natural abundance of ^{50}V (Fig. 3). Therefore both the previous data around 14.8 MeV [68–70] and the measurements carried out in this work at energies below 15 MeV correspond to the latter reaction. This conclusion is supported by the $^{50}V(n,\alpha)^{47}Sc$ cross section value deduced from the systematics at 14.8 MeV [82]. The model estimate for the $^{50}V(n,\alpha)^{47}Sc$ reaction is somewhat lower than the data between 13 and 15 MeV.

From Fig. 4(a) the overall agreement between the model calculation and the data for the $^{51}V(n,\alpha)^{48}Sc$ reaction is seen to be good. It may be noted that the data below 10 MeV are particularly insensitive to the level density model of the residual nucleus and have only a slight sensitivity to the level density of the neutron emission channel. For this reason these data were previously used to establish the OMP for α-particle emission [55]. However, the present model for the moment of inertia affects the neutron-channel level density in a more important way than was recognized in Ref. [55]. If one determines the BSFG parameters by fit to the experimental data using as an alternative $I/I_r = 1$ or $I/I_r = 0.5$ then the resulting cross section changes by 45% in this energy range. For the present assumption for the moment of inertia, the results of the OMP's of Refs. [55,83] are compared to the data below 10 MeV in Fig. 4(b). Clearly the agreement is not very good. Above 7.5 MeV the OMP of Ref. [55] agrees better with the data. Below 7.5 MeV the OMP of Ref. [83] is favored, however, the latter potential was found to be unsatisfactory when the entire energy range was considered [Fig. 4(a)]. No reasonable change to the level density model could change this conclusion so that the OMP of Ref. [55] was taken for all the final calculations of the alpha emission reactions. To improve the agreement with the data below 10 MeV one may finally consider the level scheme of ^{48}Sc. To judge the impact of the level scheme the spin assignments for the first and second excited level were altered, from 5 and 4, respectively, to 4 and 2 $\hbar$, consistent with spectroscopic information [31]. As seen from Figs. 4(a) and (b), this considerably improves agreement with the data between 8- and 10-MeV incident energy.

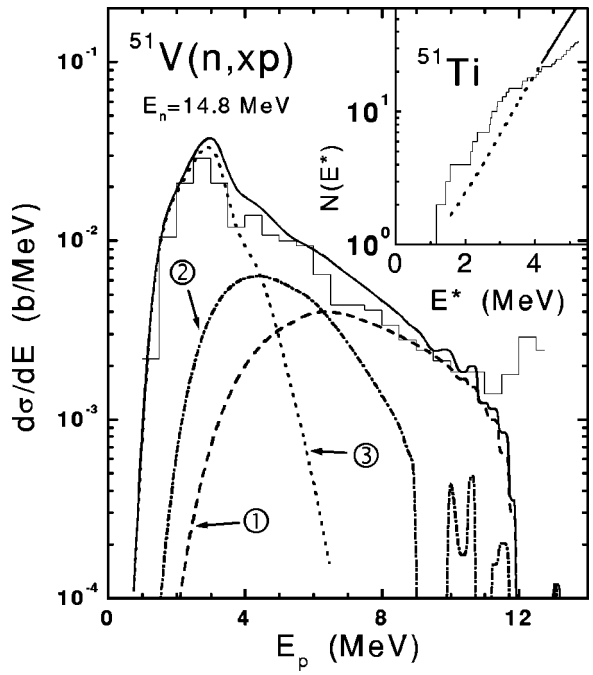

FIG. 7. Comparison of experimental [9] and calculated angle-integrated proton-emission spectra for 14.8-MeV neutron-induced reactions on ^{51}V (histogram: experiment; solid line: calculation). The various contributions are from PE emission (curve 1), first-proton statistical emission (curve 2), and second-proton statistical emission (curve 3). In the inset are shown the cumulative number of the low-lying levels [31] (histogram) of the residual nucleus ^{51}Ti for the (n,p) reaction, versus the excitation energy, and the corresponding curve given by the level density parameters involved in the model calculations (dashed in the region of the discrete low-lying levels used in HF calculation).

For the preequilibrium treatment within the GDH model, the alpha particle mean Fermi energy was taken as $\overline{F}_1^{\alpha}(R_l) = 4\overline{F}_1(R_l)$ [48], contrary to earlier work [36,84]. Through the connection with the nucleon local Fermi energy $\overline{F}_1(R_l)$ this enables surface effects for the α particle. Thus the partial wave with $l=6\ \hbar$ starts to contribute at the incident energy $\sim$12.7 MeV and gives rise to a stronger slope, whereas the next partial wave does not contribute directly below 21 MeV. The small dent seen in the calculated cross section around 15.8 MeV [Fig. 4(a)] is due to the increase of the nucleon PE emission by the $l=5\hbar$ partial wave. These preequilibrium effects help to establish good agreement with the measured data.

The analysis of α emission is completed by a comparison of the calculated and measured [9] angle-integrated emission spectra from 15 MeV neutrons on ^{51}V (Fig. 5). The experimental data are given in the laboratory system, so the comparison should be done after transformation of the measured data to the center-of-mass system. This transformation causes a shift of the measured data between 0.5 and 1 MeV to higher emission energies [85]. Taking this into account, the general agreement of experiment and model calculation is good. The experimental integrated cross section is 17 $\pm$3 mb while the calculated one is 17.3 mb.

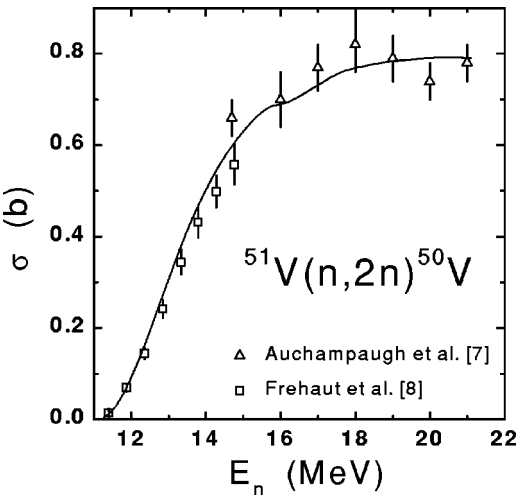

FIG. 8. Comparison of experimental and calculated cross sections of the reaction ^{51}V$(n,2n)^{50}$V. The solid line gives the result of the model calculation.

B. The (n,xp) reactions

Figure 6 shows that the excitation function of the ^{51}V$(n,p)^{51}$Ti reaction is described rather well by the present model calculation. Slight discrepancies exist. Between 4.5 and 7 MeV the model estimate is below the measured data. Most likely this is due to some of the spin and parity assignments of the 22 discrete levels used for ^{51}Ti. Between 9 and 10 MeV the model has to make the best of the slight mismatch in the measured data of Refs. [74,81] and at 20.5 MeV the model estimate is slightly higher than the data of Ref. [2].

Preequilibrium emission is particularly important for this reaction and the GDH model performs well in this case. The importance of preequilibrium contributions is demonstrated in Fig. 6(a) where two Hauser-Feshbach calculations are shown without preequilibrium contributions included. The first calculation uses the level density parameters of Table II. The second uses a modified level density parameter and back-shift for the residual nucleus. In particular, the width of the excitation curve cannot be reproduced. PE emission was also calculated with the exciton model [42] and three values for the average effective transition matrix element (the parameter FM). Broader excitation functions result compared to the Hauser-Feshbach calculations. However, the trend of the data above 15 MeV is not reproduced and the agreement with the data between 7 and 9.5 MeV is worse compared to the calculation with the GDH model [Fig. 6(a)].

The energy dependence of the preequilibrium contribution given by the GDH model is influenced by the successive openings of partial wave contributions. The latter effect is visible in Fig. 6 around 16 MeV. To understand this plateau in the calculation it is important to remember the surface effects of the GDH model. These result from the surface-peaked imaginary OMP and the use of reduced local-density Fermi energies $\overline{F}_1(R_l)$ in the finite-depth correction of the partial level densities ($R_l = l\lambda$ [40]). In the present case it is the $l=5\hbar$ partial wave for which $\overline{F}_1(R_l)$ just crosses the first hole average excitation energy resulting in a sudden increase of the PLD. Therefore the PE contribution rises suddenly

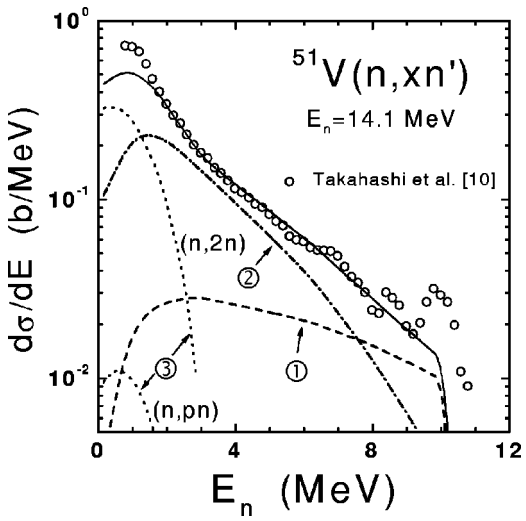

FIG. 9. Comparison of experimental [10] and calculated angle-integrated neutron-emission spectra for 14.1 MeV neutron-induced reactions on ^{51}V. The full calculation is given by the solid line. The various contributions are from PE emission (curve 1), first-neutron statistical emission (curve 2), and second-neutron statistical emission (curves 3).

around this incident energy, and leads to the appropriate behavior of the (n,p) reaction cross sections above 15 MeV. In the GDH algorithm the start of this effect of a partial wave is sharp as a consequence of the use of classical trajectories. A smoothing of the calculated cross sections is required to render the calculation physical. Here this is carried out over ~ 2 MeV around the incident energy of ~ 16 MeV. Thus a plateau is obtained.

A comparison of the experimental data [9] and the calculated angle-integrated proton spectra (this work) at the incident neutron energy of 15 MeV is shown in Fig. 7, including the calculated contributions from various processes. The agreement is good within the limits of the errors except between 11.5 and 13 MeV. The experimental integrated cross section is 91 ± 14 mb while the calculated one is 91.15 mb, in excellent agreement. The value of -1.23 MeV for the BSFG backshift in the case of the nucleus ^{51}Ti given in Table II, was needed to obtain agreement for the spectrum in the energy range where the PE contribution is dominant. Without this large negative backshift the underestimation of the experimental spectrum at the high energy end extends over a range twice as large. The agreement is improved with an even larger negative BSFG backshift Δ due to a more effective shell correction. The uncertainty of the low-lying level scheme of ^{51}Ti, with only three excited levels within ~ 800 keV above ~ 3.25 MeV, allows lower values for Δ (inset of Fig. 7). However, the change of the slope of the (n,p) reaction excitation function between 8 and 9 MeV would not be described then.

A final point in question concerns the unusual peak of the experimental proton spectrum [9] at the high energy end. This feature was also reported for the proton-emission spectrum in the case of the target nucleus ^{93}Nb in the same work [9]. It could be physically realistic since the corresponding residual nuclei have no (^{51}Ti) or only two (^{93}Zr) excited levels in the first MeV above the ground state. Even so, high population of the ground state is not common in (n,p) reactions. It is, for instance, absent in the case of ^{48}Ti(n,xp) [86]. Moreover, two other measurements for ^{93}Nb at 14.1 MeV incident energy [87,88] display the usual continuously decreasing shape approaching the ground state of the residual nucleus for the (n,p) reaction. Therefore there are too many question marks in order to derive definite conclusions on the high energy end of this proton spectrum.

C. The (n,xn') reactions

Two experimental cross-section sets [7,8] are available for the reaction ^{51}V$(n,2n)^{50}$V. They cover adjacent incident energy ranges with overlap at only one energy. At this energy a slight mismatch is observed; in general, however, a smooth trend is seen given the stated uncertainties. The calculated excitation function (Fig. 8) describes both data sets rather well. The plateau caused by the onset of the PE contribution corresponding to the partial wave with $l = 5\hbar$ is less apparent than that for the (n,p) reaction because of the indirect effect of PE emission on the $(n,2n)$ reaction. Actually the total PE emission, of which over 80% is formed by neutrons, is not greater than $\sim 28\%$ at the highest incident energy of 21 MeV involved in this work. Therefore any option of the PE model affects the $(n,2n)$ cross section only slightly. The smoothing of the calculated cross sections has been accordingly carried out over only 0.6 MeV around the incident energy of ~ 16 MeV. However, the above-mentioned plateau contributes to the change of the slope of the excitation function, which is necessary to describe its maximum around 18–20 MeV.

An analysis of the angle-integrated neutron-emission spectrum is shown in Fig. 9. The calculated spectrum has a rather sharp high-energy end which corresponds to the highest discrete level of the target nucleus ^{51}V. The contribution of the direct component estimated by the DWBA method was not added to the calculation in this graph. Here, we analyzed only the region of the spectrum corresponding to the PE and statistical emission. The agreement between the experimental [10] and calculated cross sections is good except for emission energies lower than 2 MeV. On the other hand, the very close agreement between experimental and calculated $(n,2n)$ reaction cross sections just above the threshold of the excitation function validated the low-energy neutron transmission coefficients used in this work. Therefore discrepancies between the calculated and experimental neutron-emission spectra at the lowest-energies have other reasons [89].

V. SUMMARY AND CONCLUSIONS

Cross sections for the ^{51}V$(n,p)^{51}$Ti, ^{51}V$(n,\alpha)^{48}$Sc, and $^{\text{nat}}$V$(n,x\alpha)^{47}$Sc reactions were measured in the energy range from 11.7 to 20.5 MeV. For the production of ^{47}Sc from natural vanadium this work establishes the first excitation curve. It is consistent with recent 14.8-MeV data and with a threshold behavior appropriate to the ^{51}V$(n,n'\alpha)^{47}$Sc reaction. An important consequence of this work is the conclu-

sion that the ^{47}Sc yields at 14.8 MeV must be attributed to the $^{50}V(n,\alpha)^{47}Sc$ process. Earlier work attributing this yield to the $(n,n'\alpha)$ reaction on ^{51}V, resulted in excitation curves at marked variance with the present measured data. The present result is supported by systematics for (n,α) reactions at 14.8 MeV although the measured $^{50}V(n,\alpha)$ cross section appears to be about 25% larger than expected [82]. Our results for the $^{51}V(n,\alpha)^{48}Sc$ reaction are in good agreement with the large existing data base, but suggest a slightly higher cross section above 18 MeV. The two data points added to the available experimental data for the $^{51}V(n,p)^{51}Ti$ reaction connect the recent measurements by Fessler *et al.* [2] to those by Smith *et al.* [74], Meadows *et al.* [79], Mannhart *et al.* [81], and Ikeda *et al.* [75] but disagree with Katoh *et al.* [80].

The three above mentioned excitation functions, as well as that for the competing $^{51}V(n,2n)^{50}V$ reaction are rather well described by statistical model calculations with preequilibrium contributions estimated with the GDH model in the incident energy range from threshold to 21 MeV. A consistent parameter set was used. Agreement with the data in the threshold region validates the choice of the optical model parameters of this work. In particular, in the case of α emission the potential of Ref. [55] is preferred over that of Ref. [83]. For neutrons a small change to the OMP of Ref. [4] was made, and for protons a combination of Refs. [53,52] was used with the asymmetry of Ref. [54].

It was demonstrated here that preequilibrium emission is important for the reactions studied in this work. This is most evident for the $^{51}V(n,p)^{51}Ti$ reaction above 15 MeV incident energy. However, for all excitation functions discussed here the detailed agreement that was obtained is also a result of the particular energy dependence of the pre-equilibrium contribution of the GDH model. This energy dependence is influenced significantly by the sudden opening of contributions from individual partial waves that are shown here by the calculated curves. Although the suddenness is an artifact of the semiclassical approach of the GDH, the result after smoothing is in good agreement with the data.

It was noted that because of the surface peaked nature of the imaginary OMP, the geometric nature of the GDH leads to surface effects [90]. The most recent large phenomenological analysis of surface effects in the framework of the exciton model [91] also pointed out more surface localization at lower energies (e.g., for incident neutrons up to 26 MeV). The phenomenological effective well depth and the local Fermi energies of Ref. [91], are close to those that were important for the level of agreement that was obtained in this work.

The simple but efficient GDH model, using no free parameter, could be further improved by inclusion of the average Fermi energy obtained by taking into account both the nuclear density and the first *NN*-collision probability. Finally, it would be interesting to compare the data and the GDH model description with calculations in which the onset of contributions from different partial waves to the PE process is treated in a more physical manner.

ACKNOWLEDGMENTS

One author (V.A.) is grateful to the EC/JRC for support to carry out research at the IRMM Van de Graaff laboratory during March-April 2000. This work was supported in part by the EC/JRC/IRMM, and the Contract of Association between EURATOM and NASTI-Bucharest No. ERB-5005-CT-990101. P.R. is grateful to the Commission of the European Communities for financial support.

[1] A. Fessler, E. Wattecamps, D.L. Smith, and S.M. Qaim, Phys. Rev. C **58**, 996 (1998).

[2] A. Fessler, A.J.M. Plompen, D.L. Smith, and Y. Ikeda, Nucl. Sci. Eng. **134**, 171 (2000).

[3] A.B. Smith, J.F. Whalen, and K. Takeuchi, Phys. Rev. C **1**, 581 (1970); EXFOR-10008 data file (EXFOR may be accessed online at www.nndc.bnl.gov/nndc/exfor, www.nea.fr, or www-nds.iaea.or.at/exfor), dated 1974-06-10.

[4] R.D. Lawson, P.T. Guenther, and A.B. Smith, Nucl. Phys. **A493**, 267 (1989).

[5] A. B. Smith, D. L. Smith, P. T. Guenther, J. W. Meadows, R. D. Lawson, R. J. Howerton, T. Djemil, and B. J. Micklich, *Neutronic Evaluated Nuclear Data File for Vanadium*, Argonne National Laboratory Report No. ANL/NDM-105, www.td.anl.gov/reports, Argonne, 1988.

[6] A. Brusegan, R. Shelley, G. Rohr, E. Macavero, C. Nazareth, and C. van der Vorst, in *Nuclear Data for Science and Technology*, edited by G. Reffo, A. Ventura, and C. Grandi (Editrice Compositori, Bologna, 1997), p. 410; EXFOR-22333 data file EXFOR-10008 data file (EXFOR may be accessed online at www.nndc.bnl.gov/nndc/exfor, www.nea.fr, or www-nds.iaea.or.at/exfor).

[7] G. F. Auchampaugh, D. M. Drake, L. R. Vesser, Neutron cross section programs in the energy region from 1 to 24 MeV at the LASL Van de Graaff Facilities, BNL-Brookhaven Report No. BNL-NCS-50681, 1977, p. 231.

[8] J. Frehaut, A. Bertin, R. Bois, and J. Jary, Symposium on Neutron Cross Sections from 10–50 MeV, Upton, New York, 1980; EXFOR-20416 data file EXFOR-10008 data file (EXFOR may be accessed online at www.nndc.bnl.gov/nndc/exfor, www.nea.fr, or www-nds.iaea.or.at/exfor), dated 1986-09-26.

[9] S.M. Grimes, R.C. Grimes, and J.D. Anderson, Phys. Rev. C **17**, 508 (1978).

[10] A. Takahashi, E. Ichimura, Y. Sasaki, and H. Sugimoto, Double and single differential neutron emission cross sections at 14.1 MeV, Vol. 1., Osaka University Report OKTAVIAN A-87-03, 1987.

[11] H. Vonach, M. Uhl, B. Strohmaier, B.W. Smith, E.G. Bilpuch, and G.E. Mitchell, Phys. Rev. C **38**, 2541 (1988).

[12] Handbook for calculations of nuclear reaction data, Reference Input Parameter Library, IAEA Report IAEA-TECDOC-1034 (www.nds.iaea.or.at/ripl), Vienna, 1998.

[13] M.B. Chadwick *et al.*, Nucl. Sci. Eng. **131**, 293 (1999).

[14] S.M. Qaim, M. Uhl, N.I. Molla, and H. Liskien, Phys. Rev. C **46**, 1398 (1992).
[15] D.L. Smith, J.W. Meadows, and I.C. Gomes, Fusion Eng. Des. **47**, 61 (1999).
[16] A. J. M. Plompen, P. Reimer, S. M. Qaim, A. Fessler, and D. L. Smith, Proceedings of the Physor 2000 Conference, Pittsburgh, PA, 2000, and references therein.
[17] K.J.R. Rosman and P.D.P. Taylor, Pure Appl. Chem. **70**, 217 (1998).
[18] S.M. Qaim, R. Wölfle, M.M. Rahman, and H. Ollig, Nucl. Sci. Eng. **88**, 143 (1984).
[19] A. Grallert, J. Csikai, and S.M. Qaim, Nucl. Instrum. Methods Phys. Res. A **337**, 615 (1994).
[20] I.-G. Birn, NEUT–Ein Programm zur Berechnung von Neutronenspektren erzeugt durch die $D(d,n)^3$ He-Reaktion in einem Gastarget am Zyklotron, KFA-Jülich, Internal Report No. INC-IB-1/92, 1992.
[21] I.-G. Birn, Calculation of the Mean Energy and the Energy Spread of Neutrons Produced by the $D(d,n)^3$ He Reaction in a Gas Target, CEC-JRC, IRMM, Geel, internal Report No. GE/R/VG/85/94, 1994.
[22] S. Cabral, G. Börker, H. Klein, and W. Mannhart, Nucl. Sci. Eng. **106**, 308 (1990).
[23] J. F. Briesmeister, MCNP A General Monte Carlo N-Particle Transport Code, Version 4C, LA-13709-M Manual, Los Alamos National Laboratory.
[24] H. Liskien and A. Paulsen, Nucl. Data Tables **11**, 569 (1973).
[25] H. H. Anderson and J. F. Ziegler, *Hydrogen Stopping Powers and Ranges in All Elements* (Pergamon, New York, 1977).
[26] *Nuclear Data Standards for Nuclear Measurements*, edited by H. Condé (NEA Nuclear Data Committee, Paris, 1992).
[27] P. Reimer, S. Sudár, A. J. M. Plompen, and S. M. Qaim (unpublished).
[28] I.-G. Birn and S.M. Qaim, Nucl. Sci. Eng. **116**, 125 (1994).
[29] B. Jäckel, W. Westmeier, and P. Patzelt, Nucl. Instrum. Methods Phys. Res. A **261**, 543 (1987).
[30] *Gamma- and X-Ray Spectrometry with Semiconductor Detectors*, edited by K. Debertin and R. G. Helmer (Elsevier, North-Holland, Amsterdam, 1988).
[31] C. L. Dunford and T. W. Burrows, Online Nuclear Data Service, IAEA Report IAEA-NDS-150 (www.nndc.bnl.gov/nndc/nudat; NNDC Report NNDC/ONL-95/10), IAEA, Vienna, Austria, 1995.
[32] M. Herman and G. Reffo, Comparison of exciton and multistep compound models, in IAEA Report INDC(NDS)-247/L, Vienna, 1991, p. 225.
[33] P. E. Hodgson, in *Nuclear Data for Science and Technology*, edited by S. Igarasi (Saikon, Tokyo, 1988), p. 655.
[34] P. D. Kunz, DWUCK4 user manual, OECD/NEA Data Bank, Issy-les-Moulineaux, France, 1984; www.nea.fr/abs/html/nesc9872.html
[35] T.W. Burrows, Nucl. Data Sheets **75**, 1 (1995).
[36] M. Avrigeanu, M. Ivascu, and V. Avrigeanu, Z. Phys. A **335**, 299 (1990).
[37] M. Blann, Phys. Rev. Lett. **28**, 757 (1972); Nucl. Phys. **A213**, 570 (1973); M. Blann and H.K. Vonach, Phys. Rev. C **28**, 1475 (1983).
[38] M. Avrigeanu and V. Avrigeanu, Recent improvements of the STAPRE-H95 preequilibrium and statistical model code, Institute of Physics and Nuclear Engineering Report NP-86-1995, Bucharest, 1995.
[39] M. Avrigeanu and V. Avrigeanu, J. Phys. G **20**, 613 (1994).
[40] M. Avrigeanu and V. Avrigeanu, Comput. Phys. Commun. **112**, 191 (1998); A. Harangozo, I. Stetcu, M. Avrigeanu, and V. Avrigeanu, Phys. Rev. C **58**, 295 (1998).
[41] E. Gadioli and E. Gadioli-Erba, Z. Phys. A **299**, 1 (1981).
[42] M. Uhl, Nucl. Phys. **A184**, 253 (1972); M. Uhl and B. Strohmaier, Computer Code for Particle Induced Activation Cross Section and Related Quantities, Institut für Radiumforschung und Kernphysik Report IRK 76/01, Vienna, 1976.
[43] O. Bersillon, SCAT2: Un programme de modele optique spherique, CEN-Bruyeres-le-Chatel, Note CEA-N-2227, 1981.
[44] W. Dilg, W. Schantl, H. Vonach, and M. Uhl, Nucl. Phys. **A217**, 269 (1973).
[45] A.R. Junghans, M. de Jong, H.-G. Clerc, A.V. Ignatyuk, G.A. Kudyaev, and K.-H. Schmidt, Nucl. Phys. **A629**, 635 (1998).
[46] J. P. Delaroche, Ch. Lagrange, and J. Salvy, *Nuclear theory in neutron nuclear data evaluation*, Report IAEA-190 (IAEA, Vienna, 1976), Vol. 1, p. 251.
[47] S. Cierjacks, P. Forti, D. Kopsch, L. Kropp, J. Nebe, and H. Unseld, High Resolution Total Cross Sections for Na, Cl, K, V, Mn, and Co between 0.5 and 30 MeV, OECD Report EANDC(E)-111, 1968; EXFOR-20011 data file (EXFOR may be accessed online at www.nndc.bnl.gov/nndc/exfor, www.nea.fr, or www-nds.iaea.or.at/exfor), dated 1970-12-11.
[48] E. Gadioli, E. Gadioli-Erba, J.J. Hogan, and K.I. Burns, Z. Phys. A **301**, 289 (1981).
[49] V. N. Levkovskij, Activation Cross Sections by Protons and Alphas, Moscow, 1991; EXFOR-A0510 data file (EXFOR may be accessed online at www.nndc.bnl.gov/nndc/exfor, www.nea.fr, or www-nds.iaea.or.at/exfor), dated 1993-04-15.
[50] H. I. West, Jr., R. G. Lanier, and M. G. Mustafa, Excitation functions for the nuclear reactions on titanium leading to the production of ^{48}V, ^{44}Sc, and ^{47}Sc, by proton, deuteron and triton irradiations at 0-35 MeV, Report UCRL-ID-115738, Livermore, 1993.
[51] A. E. Antropov, P. P. Zarubin, Yu. A. Aleksandrov, and I. Yu. Gorshkov, 35th Conference on Nuclear Spectroscopy and Nuclear Structure, Leningrad, 1985; EXFOR-O0076 data file (EXFOR may be accessed online at www.nndc.bnl.gov/nndc/exfor, www.nea.fr, or www-nds.iaea.or.at/exfor), dated 1995-02-14.
[52] S. Kailas, M.K. Mehta, S.K. Gupta, Y.P. Viyogi, and N.K. Ganguly, Phys. Rev. C **20**, 1272 (1979).
[53] F.G. Perey, Phys. Rev. **131**, 745 (1963).
[54] D. M. Hetrick, C. Y. Fu, and D. C. Larson, Calculated neutron-induced cross sections for ^{63,65}Cu from 1 to 20 MeV and comparisons with experiments, Oak Ridge National Laboratory Report ORNL/TM-9083, Oak Ridge, 1984.
[55] V. Avrigeanu, P.E. Hodgson, and M. Avrigeanu, Phys. Rev. C **49**, 2136 (1994).
[56] C.H. Johnson, Phys. Rev. C **16**, 2238 (1977).
[57] S.F. Mughabghab and C. Dunford, Phys. Rev. Lett. **81**, 4083 (1998).
[58] B.K. Agrawal, S.K. Samaddar, A. Ansari, and J.N. De, Phys. Rev. C **59**, 3109 (1999).

[59] H. Weigmann, C. Wagemans, A. Emsallem, and M. Asghar, Nucl. Phys. **A368**, 117 (1981).
[60] D.J. Dean, S.E. Koonin, K. Langanke, P.B. Radha, and Y. Alhassid, Phys. Rev. C **74**, 2909 (1995).
[61] B.K. Agrawal, S.K. Samaddar, J.N. De, and S. Shlomo, Phys. Rev. C **58**, 3004 (1998).
[62] B.K. Agrawal and A. Ansari, Phys. Lett. B **421**, 13 (1998).
[63] A.J. Koning and M.B. Chadwick, Phys. Rev. C **56**, 970 (1997).
[64] P. Möller, J.R. Nix, W.D. Myers, and W.J. Swiatecki, At. Data Nucl. Data Tables **59**, 185 (1995).
[65] A.S. Iljinov, M.V. Mebel, N. Bianchi, E. de Sanctis, C. Guaraldo, V. Lucherini, V. Muccifora, E. Polli, A.R. Reolon, and P. Rossi, Nucl. Phys. **A543**, 517 (1992).
[66] M. Bormann, S. Cierjacks, R. Langkau, H. Neuert, and H. Pollehn, J. Phys. Radium **22**, 602 (1961).
[67] M. Bormann, S. Cierjacks, R. Langkau, and N. Neuert, Z. Phys. **166**, 477 (1962).
[68] R. Pepelnik, B. Anders, and B. M. Bahal, in Proceedings of the International Conference on Nuclear Data for Basic and Applied Science, Santa Fe, 1985, edited by P. G. Young, R. E. Brown, G. F. Auchampaugh, P. L. Lisowski, and L. Stewart, p. 211.
[69] S.M. Qaim, Nucl. Phys. **A458**, 237 (1986).
[70] A. Grallert, J. Csikai, C. M. Buczkó, and I. Shaddad, Investigations on the systematics in (n,α) cross sections at 14.6 MeV, IAEA Report INDC(NDS)-286, Vienna, 1993, p. 131.
[71] Wang Yongchang, Yang Jingkang, Yuan Junqian, and Kong Xiangzhong, Chinese J. High Energy Phys. Nucl. Phys. **17**, 290 (1993); EXFOR-32515 data file (EXFOR may be accessed online at www.nndc.bnl.gov/nndc/exfor, www.nea.fr, or www-nds.iaea.or.at/exfor), dated 1999-07-17.
[72] A. Paulsen, R. Widera, and H. Liskien, Atomkernenergie **22**, 291 (1974).
[73] E. Zupranska, K. Rusek, J. Turkiewicz, and P. Zupranski, Acta Phys. Pol. B **11**, 853 (1980); EXFOR-30581 data file (EXFOR may be accessed online at www.nndc.bnl.gov/nndc/exfor, www.nea.fr, or www-nds.iaea.or.at/exfor), dated 1984-09-11.
[74] D.L. Smith, J.W. Meadows, and I. Kanno, Ann. Nucl. Energy **11**, 623 (1984).
[75] Y. Ikeda, C. Konno, K. Oishi, T. Nakamura, H. Miyade, K. Kawade, H. Yamamoto, and T. Katoh, Activation Cross Section Measurements for Fusion Reactor Structural Materials at Neutron Energies from 13.3 to 15.0 MeV using FNS Facility, Report JAERI-1312, 1988.
[76] Lu Han-Lin, Wang Da-Hai, Xiu Yi-Jun, Cui Yun-Fang, and ChenPao-Lin, Excitation Curves for some Reactions of Al, Ti, V, and I, IAEA Report INDC(CPR)-16, Vienna, 1989.
[77] R. Doczi, V. Semkova, A. Fenyvesi, N. Yamamuro, Cs.M. Buczko, and J. Csikai, Nucl. Sci. Eng. **129**, 164 (1998).
[78] A. A. Filatenkov *et al.*, Systematic Measurement of Activation Cross Sections at Neutron Energies from 13.4 to 14.9 MeV, IAEA Report INDC(CCP)-402, Vienna, 1997; Khlopin Radium Institute Report RI-252, St. Petersburg, 1999.
[79] J.W. Meadows, D.L. Smith, M.M. Bretscher, and S.A. Cox, Ann. Nucl. Energy **14**, 489 (1987).
[80] T. Katoh, K. Kawade, and H. Yamamoto, Measurement of Activation Cross Sections, Report JAERI-M-89-026, 293, 1989.
[81] W. Mannhart, D. Schmidt, and D. L. Smith, in *Nuclear Data for Science and Technology*, edited by G. Reffo, A. Ventura, and C. Grandi (Editrice Compositori, Bologna, 1997), p. 505.
[82] A. D. Majdeddin, V. Semkova, R. Dóczi, Cs. M. Buczkó, and J. Csikai, Investigations on (n,α) Cross Sections in the 14 MeV Region, IAEA Report INDC(HUN)-031, Vienna, 1993.
[83] L. McFadden and G.R. Satchler, Nucl. Phys. **A84**, 177 (1966).
[84] M. Avrigeanu, P. E. Hodgson, V. Avrigeanu, and A. Harangozo, in *Proceedings of the International Conference on Nuclear Data for Science and Technology*, Gatlinburg, Tennessee, 1994, edited by J. K. Dickens (American Nuclear Society, La Grange Park, 1994), p. 476.
[85] R. Fischer, G. Traxler, M. Uhl, and H. Vonach, Phys. Rev. C **30**, 72 (1984).
[86] S.M. Grimes, R.C. Haight, and J.D. Anderson, Nucl. Sci. Eng. **62**, 187 (1977).
[87] N. Koori, Y. Ohsawa, and I. Kumabe, Nucl. Sci. Eng. **87**, 34 (1984).
[88] G. Traxler, A. Chalupka, R. Fischer, B. Strohmaier, M. Uhl, and H. Vonach, Nucl. Sci. Eng. **90**, 174 (1985).
[89] A.A. Kychagin *et al.*, Yad. Fiz. **45**, 1226 (1987).
[90] M. Avrigeanu, A. Harangozo, V. Avrigeanu, and A.N. Antonov, Phys. Rev. C **54**, 2538 (1996).
[91] C. Kalbach, Phys. Rev. C **62**, 044608 (2000).